Chapter 2

Materials, Methods and Instrumentation

This chapter includes the information of chemicals and reagents used for the synthesis of imidazolium- and pyridinium-based compounds as well as for catalytic and chemosensory applications. Details of different instrumentation techniques employed for the characterization and study of the photophysical properties of synthesized compounds are discussed.

2.1 Chemicals and reagents

List of chemicals and reagents used for the synthesis, catalytic, and sensing applications purchased from different suppliers are given below:

Alfa Aesar Pvt. Ltd.

1,2-Diaminobenzene, 2,4-dihydroxybenzaldehyde, 2-aminochlorobenzene, 4-chlorotoluene, 4-chloroanisole, 3,4-dimethoxyboronic acid, 1-fluoro-2-iodobenzene, 1-iodo-4-nitrobenzene, 2-iodoaniline, 1-iodo-2-nitrobenzene, 4-nitrochlorobenzene, 2-nitrochlorobenzene, 2,3,4-trimethoxyboronic acid, 3,4,5-trimethoxyboronic acid.

Sigma Aldrich Pvt. Ltd.

8-Aminoquinoline, 1-methylimidazole, palladium(II) acetate, 2-chloroanisole, 2-chloropyrazine, 1-chloro-4-iodobenzene, palladium(II) acetate, 3,4-dinitrotoluene, 3,5-dinitrobenzoic acid, 3,5-dinitrotoluene, gadolinium(III) nitrate hexahydrate, 4-nitrobenzoic acid, 4-nitrotoluene palladium(II) acetate, ytterbium(III) nitrate pentahydrate.

Merck Ltd. India

Aluminium(III) nitrate nonahydrate, cadmium(II) nitrate tetrahydrate, chromium(III) nitrate nonahydrate, calcium(II) nitrate tetrahydrate, cobalt(II) nitrate hexahydrate, copper(II) nitrate trihydrate, ferric(III) nitrate nonahydrate, ferrous(II) sulfate heptahydrate, lead(II) nitrate, lanthanum(III) nitrate hexahydrate, mercury(II) nitrate monohydrate, magnesium(II) nitrate hexahydrate, manganese(II) nitrate tetrahydrate, nickel(II) nitrate hexahydrate, potassium(I) nitrate, sodium(I) nitrate, silver nitrate, zinc(II) nitrate hexahydrate**,** acetone, acetonitrile (ACN), chloroform ($CHCl_3$), dioxane, dichloromethane (DCM), dimethylformamide (DMF), dimethylsulfoxide (DMSO), ethanol (EtOH), ethyl acetate (EtOAc), ether, hexane, methanol (MeOH), and tetrahydrofuran (THF)**,** DMSO (UV-grade), MeOH (UV-grade).

Spectrochem Pvt. Ltd.

Bromoacetic acid, 1,3-dibromopropane, 1,2-dibromoethane, ethyl chloroformate, ethylenediamine, isatin, nickel(II) acetate tetrahydrate, pyridine, potassium carbonate, sodium hydrogen carbonate, sodium sulfate, triethylamine, 2-chloropyridine, 4-chloroacetophenone, 2,6-dichloropyrazine, 4-iodotoluene, 4-iodoanisole, 2-methylphenylboronic acid, 4-methoxyboronic acid, napthene-1-boronic acid, phenanthrene-9-boronic acid, phenylboronic acid, benzoic acid, 1-chloro-2,4-dinitrobenzene, 2,4-dinitrophenol, europium(III) nitrate,4-nitrophenol, nitrobenzene, nitromethane, potassium carbonate, sodium sulfate, triethylamine, tetrabutylammonium acetate, tetrabutylammonium chloride, tetrabutylammonium bromide, tetrabutylammonium hydrogen sulfate, tetrabutylammonium fluoride, tetrabutylammonium iodide, 2,4,6-trinitrophenol.

The synthesis of benzenesulfonylhydrazide, 4-methylbenzenesulfonohydrazide, 4-nitrobenzenesulfonohydrazide, naphthalene-1-sulfonohydrazide, 4-(*tert-butyl*)-benzenesulfonohydrazide and phenylmethanesulfonohydrazide were performed according to the literature procedures. [1] Deuterated DMSO and $CDCl_3$ solvents were used for ^{1}H and ^{13}C NMR analysis.

2.2 Methods

2.2.1 Detection limit calculation

The ability to quantify the lowest amount of analyte using specific analytical methods are often expressed in terms of the detection limit. This detection limit is a number, expressed in units of concentration, that describes the lowest concentration level of the analyte that can be detected under the given experimental conditions. The detection limit is calculated using the equation as given below [2-3]

$$\text{Detection limit} = 3\sigma/\text{k}$$

where σ is the standard deviation of blank measurements, k is the slope between the plot of fluorescence intensity versus sample concentration. To determine the signal/noise ratio, the fluorescence intensity of chemosensor in water without analyte was measured 10 times and the standard deviation of blank measurements is determined.

2.2.2 Fluorescence quantum yield calculation

The quantum yield of a radiation-induced process is the number of emitted photons relative to the number of absorbed photons. The relative fluorescence quantum yield calculations are performed using quinine sulfate as a reference in 0.1 M H_2SO_4 ($\Phi_R = 0.54$) using the equation as given below [4-5]

$$\Phi_S = \Phi_R \frac{I_S}{I_R} \times \frac{A_R}{A_S} \times \frac{\eta_S^2}{\eta_R^2}$$

where I = integrated area under the fluorescence curve, A = absorbance at the excitation wavelength, η = refractive index of the medium, and Φ = fluorescence quantum yield. Subscripts S and R refer to the 'sample' and the 'reference standard', respectively.

2.2.3 Binding constant calculation

The binding constant (K_B) is associated with the binding of donor and acceptor molecules and its high value suggests a strong binding. The binding constant (K_B) is calculated using the modified Benesi-Hildebrand (B-H) equation as given below [6]

$$\frac{1}{I - I_0} = \frac{1}{I_{max} - I_0} + \frac{1}{K_B(I_{max} - I_0)} \frac{1}{[\text{analyte}]^n}$$

where I_0 and I are the fluorescence intensities of chemosensor in the absence and presence of the analyte, respectively. I_{max} is the maximum fluorescence intensity of chemosensors in the presence of an analyte. n is the number of analyte molecules interacting with chemosensor.

2.2.4 Fluorescence lifetime calculation

The fluorescence lifetime is a measure of the time that a fluorophore spends in the excited state before returning to the ground state by emitting a photon. Average fluorescence lifetimes (τ_{avg}) are calculated from the decay times and pre-exponential factors using the equation as given below [7]

$$\tau_{avg} = \frac{\sum \alpha_i \tau_i^2}{\sum \alpha_i \tau_i}$$

where α_i is the pre-exponential factor corresponding to the *i*th decay time constant, τ_i.

2.2.5 Fluorescence quenching percentage calculation

Fluorescence quenching refers to any process that decreases the fluorescence intensity of a sample. A variety of molecular interactions like excited-state reactions, molecular rearrangements, ground-state complex formation, etc. can result in quenching. The quenching percentage is calculated using the equation as given below [8]

$$\text{Fluorescence quenching } \% = \left(1 - \frac{I}{I_0}\right) \times 100\%$$

where I_0 and I are the fluorescence intensities of chemosensor in the absence and presence of the analyte, respectively.

2.2.6 Stern-Volmer quenching constant calculation

Collisional quenching occurs when an excited fluorophore comes in contact with a quencher that can facilitate non-radiative transitions to the ground state. The Stern-Volmer equation can be derived by considering fluorescence intensities observed in the absence and presence of quencher. The fluorescence intensity observed for a fluorophore is proportional to its concentration in the excited state. The Stern-Volmer quenching constant (K_{SV}) is obtained using the equation as given below [9]

$$I_0/I = 1 + K_{SV}[Q]$$

where I_0 and I are the fluorescence intensities of chemosensor in the absence and presence of analyte, respectively, [Q] is the concentration of analytes.

2.2.7 Overlap integral and Förster distance calculation

The fluorescence emission spectrum of the donor molecule must overlap the absorption or excitation spectrum of the acceptor molecule. The degree of overlap is referred to as spectral overlap integral (J). R_0 is the Förster radius at which half of the excitation energy of the donor is transferred to the acceptor molecule. Overlap integral values for all analytes are calculated using the equation as given below [10]

$$J_\lambda = F_D(\lambda)\varepsilon_A(\lambda)\lambda^4 d\lambda$$

where $F_D(\lambda)$ denotes the corrected fluorescence intensity of donor in the range of λ to $\lambda + \Delta\lambda$ with the total intensity normalized to unity. ε_A is the molar absorptivity of the acceptor at λ in M^{-1} cm^{-1}.

The Förster distance R_0 is also calculated for chemosensor-analyte interaction using the expression

$$R_0 = 0.211\,[(J)Q\,(\eta^{-4})(\kappa^2)]^{1/6}$$

where J_λ is the degree of spectral overlap between the donor fluorescence spectrum and the acceptor absorption spectrum. Q = fluorescence quantum yield of the donor (without acceptor). η = the refractive index of the medium, κ^2 = 0.667: dipole orientation factor.

2.3 Instrumentation

2.3.1 Infrared (IR) spectroscopy

The infrared spectrum can be divided into three main regions: the far-infrared (<400 cm^{-1}), the mid-infrared (4000-400 cm^{-1}), and the near-infrared (13000-4000 cm^{-1}). IR radiations on interaction with a molecule cause group of atoms to vibrate with respect to the bonds that connect them. Absorption of radiation by a molecule results in the excitation of vibrational, rotational, and bending modes that alter the state of the atoms within the molecule. These changes are usually evident in alterations to the frequency and amplitude of molecular vibrations and plotted to produce an infrared spectrum. The IR spectrum is a plot of transmitted or absorbed frequencies (x-axis) *vs* intensity of the transmission or absorption (y-axis). Each molecule is a unique combination of atoms and two different compounds cannot produce the same infrared spectrum. The region from 4000-400 cm^{-1} provides structural information for most of the organic molecules and region 400-33 cm^{-1} is used for inorganic molecules. For the molecule to be 'IR active', a change in dipole moment should occur for vibration to absorb infrared energy. The basics of vibrational spectroscopy are governed by Hooke's law which states that for two-body harmonic oscillator, the frequency of vibration is

$$\overline{\nu} = \frac{1}{2\pi c}\sqrt{\frac{k}{\mu}}$$

Where, c = speed of light, k = force constant, (5 x 10^5 dynes/cm for single bond and approximately two and three times this value for the double and triple bonds, respectively) and μ = reduced mass ($m_1.m_2/m_1+m_2$). The Hooke's law is used to theoretically calculate the approximate stretching frequency of a bond [11-12]. In this thesis work, infrared spectra (4000-450 cm^{-1}) of imidazolium- and pyridinium-based ligands and their metal complexes

were recorded on ABB Bomen MB 3000 (with KBr pellets) and Perkin Elmer Spectrum 100 FTIR spectrometer (**Figure 2.1**).

Figure 2.1 Photograph of the FTIR spectrometer (a) ABB Bomen MB 3000 and (b) Perkin Elmer Spectrum 100

2.3.2 UV-Visible spectroscopy

This absorption spectroscopy ranges from 190 nm to 800 nm of electromagnetic radiations and is used to study the electronic structure and its dynamics in atoms and molecules. Energy absorbed in the UV region produces changes in the electronic energy of the molecule and promotes the electrons from their ground state to a high energy excited state. These electronic transitions result in the form of absorption bands at a particular wavelength indicating the presence of a chromophore. However, the position of the absorption band is not fixed but depends on the molecular environment of the chromophore and on the solvent polarity in which the sample is dissolved. pH and temperature may also influence the intensity and the wavelength of the absorption band.

The absorption of light in this spectroscopy can be explained according to Beer-Lambert's Law, which states that the fraction of incident radiation absorbed (A) is directly proportional to the concentration (*c)* of the species and path length (*l*) of the light passing through the sample.

$$A = \log(I_0/I) = \varepsilon . c . l$$

where, I_0 and I are the intensities of the incident and transmitted light, respectively and ε is molar absorptivity or molar extinction coefficient. Several organic compounds, as well as metal complexes, can be studied by the electronic spectroscopy[13-14].

In present work, the UV-visible spectra were recorded both in solution and solid states. The studies were performed using the Shimadzu Spectrophotometer with model UV-2450 and JASCO with model V-650 (**Figure 2.2**).

Figure 2.2 Photograph of the UV-visible spectrophotometers (a) Shimadzu UV-2450 (b) JASCO V-650

2.3.3 Nuclear Magnetic Resonance spectroscopy

Nuclear magnetic resonance **(**NMR**)** spectroscopy is used to determine the chemical and structural information of organic compounds. NMR spectroscopy involves the change in the spin state of a nucleus when it absorbs radiofrequency in a strong magnetic field. A nucleus with unpaired protons or neutrons e.g. ^{1}H, ^{3}H, ^{13}C, ^{15}N, ^{19}F, ^{31}P when placed in a powerful magnetic field absorbs electromagnetic radiation at a particular frequency and starts resonating along with or opposite to the applied magnetic field. The absorbed energy, resonance frequency, and the strength of signal intensity are directly proportional to the applied magnetic field [15-16]. The chemical shifts δ are reported in parts per million (ppm) and referred to the internal standard TMS set as 0.00 ppm, relative to residual chloroform (7.26 ppm and 77.0 ppm) or DMSO (2.5 ppm and 39.5 ppm). The following abbreviations were used to describe peak splitting patterns: s = singlet, d = doublet, t = triplet, dd = doublet of doublet and m = multiplet.

In present work, the ^{1}H, ^{13}C NMR, ^{1}H-^{1}H homonuclear correlation spectroscopy (COSY) and ^{1}H-^{13}C heteronuclear correlation spectroscopy (HETCOR) spectra of synthesized compounds

were measured on a 400 MHz NMR spectrometer (Bruker Ascend^{TM} 400) (**Figure 2.3**) using $CDCl_3$ and DMSO-d_6 as deuterated solvents.

Figure 2.3 Photograph of 400 MHz NMR spectrometer (Bruker Ascend^{TM} 400)

2.3.5 Fluorescence spectroscopy

Fluorescence spectroscopy analyzes the fluorescence resulting from the excitation of electron on the absorption of light from a sample. Fluorescence spectrometry can record both an excitation spectrum and/or an emission spectrum. In spectrofluorometer, the sample gets irradiated with excitation light and the fluorescence emitted from the irradiated sample is then measured. The intensity of the emission is directly proportional to the concentration of the analyte. In fluorescence spectroscopy, the fluorophores play a crucial role and the interactions of these fluorophores with light are investigated. The fluorophore is a molecule that absorbs the energy of a specific wavelength and then re-remits this energy at a different but equally specific wavelength [17-18]. In this thesis, the Steady-state fluorescence measurements were conducted on Horiba Jobin Yvon Fluoromax-4 scanning spectrofluorometer (**Figure 2.4**). The

quartz cuvettes of 1 cm path length, excitation, and emission slit widths of 3 nm were used for spectral measurements.

Figure 2.4 Photograph of spectrofluorometer (Horiba Jobin Yvon Fluoromax-4)

2.3.6 Time-resolved spectroscopy

Time-resolved or fluorescence lifetime spectroscopy is an extension of the steady-state fluorescence technique used to study the dynamics of short-lived intermediate species. In a time-resolved fluorescence experiment, a sample is excited by a pulsed laser and resulting emissions, and their decay times are then monitored as a function of time, either by an ultrafast detector or the second pulse of laser light. It is possible to study the decay processes that occur on ultrashort time scales (~10^{-6}-10^{-16} seconds) with the help of lasers [19-20]. In the present thesis, the fluorescence lifetime measurements were performed by time-correlated single-photon counting (TCSPC) method using Edinburgh FL920 Fluorescence Lifetime Spectrometer (**Figure 2.5**).

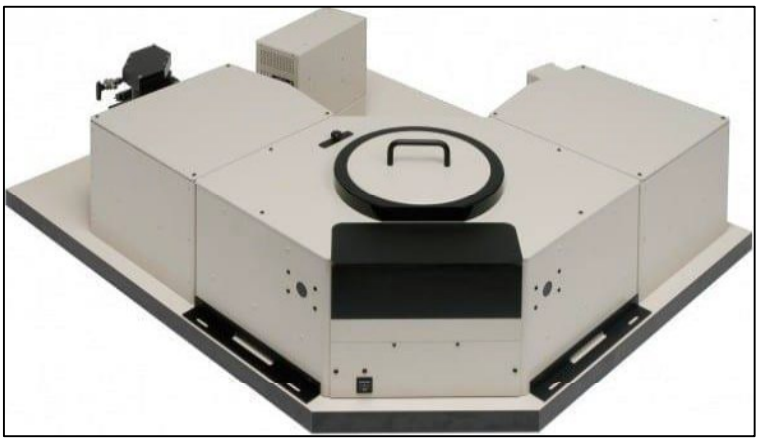

Figure 2.5 Photograph of Fluorescence Lifetime Spectrometer (Edinburgh FL920)

2.3.4 Mass spectrometry

Mass spectrometry is an analytical technique used to measure molecular or atomic weight. It has been also widely used for the monitoring of reactions. The process involves the conversion of the sample into gaseous ions, with or without fragmentation. The ions are then separated in the mass spectrometer according to their mass to charge ratio (*m/z*) and are detected qualitatively and quantitatively based on their *m/z* and relative abundance. The results are displayed in the form of a plot of ion abundance versus mass-to-charge ratio. Q-TOF (Quadrupole Time-of-Flight) LC-MS provides high-resolution mass information to the sub-ppm levels. In Q-TOF, the ions are held in a stable orbit by an electric field generated by four parallel electrodes, and the ions with different masses are accelerated to the same kinetic energy and the time taken by each ion to reach a detector at a known distance is measured. The coupling of a quadrupole and a collision cell to the TOF analyzer enhances the degree of selectivity by allowing the fragmentation of pre-selected ions and the detection of compounds based on their product ion spectra. Hence the accurate mass determination of both the precursor and product ions is, therefore, possible [21-23]. In the present thesis, the mass spectra for different synthesized compounds and reaction intermediates were recorded on 6545 Q-TOF LC/MS, Model-G6545A (**Figure 2.6**).

Figure 2.6 Photograph of mass spectrometer (6545Q-TOF LC/MS)

2.3.7 Single-crystal X-ray diffraction

Single-crystal X-ray diffraction is an analytical technique that provides detailed information about crystal structures and atomic spacing. The unit cell dimensions, bond-lengths, bond-angles can be deduced by this technique. X-ray diffraction is based on the constructive interference of monochromatic X-rays and a crystal sample. The interaction of the incident rays with the sample generates constructive interference (and a diffracted ray) when conditions satisfy the Bragg's Law ($n\lambda = 2d\sin\theta$). This law relates the wavelength of electromagnetic radiation to the diffraction angle and the lattice spacing in a crystal sample. By changing the geometry of the incident rays, the alignment of the centred crystal and the detector, all possible diffraction paths of the lattice are attained. The main component of all diffraction is the angle between the incident and diffracted rays [24-26]. The single-crystal XRD data were collected on a Rigaku-Oxford XtaLAB Pro: Kappa dual home/near diffractometer (**Figure 2.7**) with CCD detector and fine focus sealed X-ray tube monochromated MoKα/CuKα radiations. The suitable crystals were kept at 293 K during data collection. The data collection and data reduction were performed with CrysAlisPro software. The structures were solved using Olex2 [27] with ShelXT [28] structure solution program using Intrinsic Phasing and refined with the ShelXL [29] refinement package using Least Squares minimization.

Figure 2.7 Photograph of Single-crystal X-ray diffractometer (Rigaku-Oxford XtaLAB)

2.3.8 Microwave synthesis

Microwave radiation is generally defined as that part of the electromagnetic spectrum with frequencies 0.3-300 GHz. All microwave reactors for chemical synthesis operate at a frequency of 2.45 GHz to avoid interference with cellular phone and telecommunication frequencies. For microwave heating, the substance must possess a dipole moment. A dipole is sensitive to the external electric field and tries to align itself with the field by rotation. The microwaves directly couple with the molecules of the entire reaction mixture leading to the rapid increase in temperature. Only the reaction vessel contents are heated and not the vessel itself providing better homogeneity and selective heating of polar molecules. The reactions under microwaves are fast, with increased reaction rates, and lead to better selectivity [30-31]. In this thesis, the microwave reactions were performed in a Monowave 300 (Anton Paar, Austria) microwave synthesis reactor (**Figure 2.8**) with 10 mL standard vials and Teflon-coated magnetic stir bar.

Figure 2.8 Photograph of microwave synthesis reactor (Monowave 300, Anton Paar)

2.3.9 Computational study

The computational or theoretical study is a method to investigate the structural, electronic, and magnetic properties of molecules and materials. Computational results can be used to support the information obtained by chemical experiments, and in some cases predict previously ignored chemical phenomena. It is widely used for designing new drugs and materials. In the present thesis, all the computational calculations were done on the Gaussian09 package [32]. For geometry optimization, density functional theory (DFT) method was used at B3LYP (Becke three-parameter exchange functional [33] and Lee-Yang-Parr correlation functional [34] level and standard 6-31+G(d,p) and 6-311+G(d,p) for C, H, N, O and Br atoms and

LANL2DZ as effective core potential (ECP) set for metal ions. TDDFT calculations were performed using the integral equation formalism-polarizable continuum model (IEF-PCM) [35] with the same B3LYP level and basis sets using water as a solvent medium. For the optimized geometries, no imaginary frequencies were observed.

2.4 References

[1] Backes, G. L.; Neumann, D. M.; Jursic, B. S. *Bioorganic & Medicinal Chemistry* **2014**, *22*, 4629-4636.

[2] Kaur, I.; Sharma, V.; Mobin, S. M.; Kaur, P.; Singh, K. *Sensors and Actuators B: Chemical* **2019**, *281*, 613-622.

[3] Forootan, A.; Sjöback, R.; Björkman, J.; Sjögreen, B.; Linz, L.; Kubista, M. *Biomolecular Detection and Quantification* **2017**, *12*, 1-6.

[4] Chao, D. *Journal of Chemical Sciences* **2016**, *128*, 133-139.

[5] Luo, T.; Li, Y.; Xu, Y.; Zhang, S.; Wang, Y.; Kou, X.; Xiao, D. *Sensors and Actuators B: Chemical* **2017**, *253*, 231-238.

[6] Tian, J.; Yan, X.; Yang, H.; Tian, F. *RSC Advances* **2015**, *5*, 107012-107019.

[7] Naskar, B.; Bauzá, A.; Frontera, A.; Maiti, D. K.; Das Mukhopadhyay, C.; Goswami, S. *Dalton Transactions* **2018**, *47*, 15907-15916.

[8] Joshi, S.; Kumari, S.; Chamorro, E.; Pant, D. D.; Sakhuja, R. *ChemistrySelect* **2016**, *1*, 1756-1762.

[9] Wahba, M. E. K.; El-Enany, N.; Belal, F. *Analytical Methods* **2015**, *7*, 10445-10451.

[10] Hussain, S.; Malik, A. H.; Afroz, M. A.; Iyer, P. K. *Chemical Communications* **2015**, *51*, 7207-7210.

[11] Stuart, B., *Infrared Spectroscopy*. Wiley Online Library: **2005**.

[12] Anderson, R. J.; Bendell, D. J.; Groundwater, P. W., *Organic spectroscopic analysis*. Royal Society of Chemistry: **2004**.

[13] Ojeda, C. B.; Rojas, F. S. *Applied Spectroscopy Reviews* **2009**, *44*, 245-265.

[14] Ozaki, Y.; Tanabe, I. *Analyst* **2016**, *141*, 3962-3981.

[15] Silverstein, R. M.; Webster, F. X., *Spectrometric Identification of Organic Compounds*. John Wiley & Sons: **2005**.

[16] Lambert, J. B.; Mazzola, E. P.; Ridge, C. D., *Nuclear magnetic resonance spectroscopy: an introduction to principles, applications, and experimental methods*.

John Wiley & Sons: **2019**.

[17] Lakowicz, J., *Spectroscopy, Principles of Fluorescence*. Springer Publications: **2006**.

[18] Albani, J. R., *Principles and applications of fluorescence spectroscopy*. John Wiley & Sons: **2008**.

[19] Stolow, A.; Bragg, A. E.; Neumark, D. M. *Chemical Reviews* **2004**, *104*, 1719-1758.

[20] Goodson, T. *Annual Review of Physical Chemistry* **2004**, *56*, 581-603.

[21] DeTata, D.; Collins, P.; McKinley, A. *Forensic Science International* **2013**, *233*, 63-74.

[22] Meyer, M. R.; Maurer, H. H. *Analytical and Bioanalytical Chemistry* **2012**, *403*, 1221-1231.

[23] Nizkorodov, S. A.; Laskin, J.; Laskin, A. *Physical Chemistry Chemical Physics* **2011**, *13*, 3612-3629.

[24] Suryanarayana, C.; Norton, M. G., *X-ray diffraction: a practical approach*. Springer Science & Business Media: **2013**.

[25] Artioli, G.; Monaco, H. L.; Viterbo, D.; Ferraris, G.; Gilli, G.; Zanotti, G.; Catti, M., *Fundamentals of crystallography*. Oxford University Press: **2002**.

[26] Boffa Ballaran, T.; Kurnosov, A.; Trots, D. *High Pressure Research* **2013**, *33*, 453-465.

[27] Dolomanov, O. V.; Bourhis, L. J.; Gildea, R. J.; Howard, J. A. K.; Puschmann, H. *Journal of Applied Crystallography* **2009**, *42*, 339-341.

[28] Sheldrick, G. M. *Acta crystallographica. Section A, Foundations and advances* **2015**, *71*, 3-8.

[29] Sheldrick, G. *Acta Crystallographica Section C* **2015**, *71*, 3-8.

[30] Tierney, J.; Lidström, P., *Microwave assisted organic synthesis*. John Wiley & Sons: **2009**.

[31] de la Hoz, A.; Loupy, A., *Microwaves in organic synthesis*. John Wiley & Sons: **2013**.

[32] Frisch, M. J.; Trucks, G. W.; Schlegel, H. B.; Scuseria, G. E.; Robb, M. A.; Cheeseman, J. R.; Scalmani, G.; Barone, V.; Mennucci, B.; Petersson, G. A.; Nakatsuji, H.; Caricato, M., *et al.*, Gaussian 09, Revision C.01. Gaussion, Inc.. Wallingford CT, **2009**.

[33] Becke, A. D. *The Journal of Chemical Physics* **1993**, *98*, 5648-5652.

[34] Lee, C.; Yang, W.; Parr, R. G. *Physical Review B* **1988**, *37*, 785-789.

[35] Tomasi, J.; Mennucci, B.; Cammi, R. *Chemical Reviews* **2005**, *105*, 2999-3094.